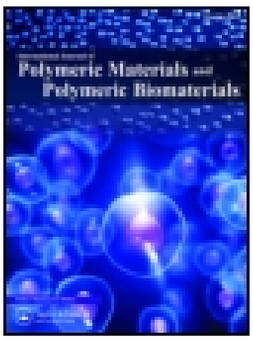

International Journal of Polymeric Materials and Polymeric Biomaterials

ISSN: 0091-4037 (Print) 1563-535X (Online) Journal homepage: https://www.tandfonline.com/loi/gpom20

New nanostructure based on hydroxyapatite modified cellulose for bone substitute, synthesis, and characterization

F. E. Tabaght, K. Azzaoui, A. Elidrissi, O. Hamed, E. Mejdoubi, S. Jodeh, N. Akartasse, M. Lakrat & A. Lamhamdi

To cite this article: F. E. Tabaght, K. Azzaoui, A. Elidrissi, O. Hamed, E. Mejdoubi, S. Jodeh, N. Akartasse, M. Lakrat & A. Lamhamdi (2020): New nanostructure based on hydroxyapatite modified cellulose for bone substitute, synthesis, and characterization, International Journal of Polymeric Materials and Polymeric Biomaterials

To link to this article: https://doi.org/10.1080/00914037.2020.1725758

Published online: 24 Feb 2020.

INTERNATIONAL JOURNAL OF POLYMERIC MATERIALS AND POLYMERIC BIOMATERIALS
https://doi.org/10.1080/00914037.2020.1725758

New nanostructure based on hydroxyapatite modified cellulose for bone substitute, synthesis, and characterization

F. E. Tabaght[a], K. Azzaoui[b], A. Elidrissi[a], O. Hamed[c], E. Mejdoubi[b], S. Jodeh[c], N. Akartasse[b], M. Lakrat[b], and A. Lamhamdi[b,d]

[a]Faculty of Sciences, Laboratory LCAE-URAC18, Mohamed 1st University, Oujda, Morocco; [b]Department of Chemistry, Faculty of Sciences, Laboratory of Mineral Solid and Analytical Chemistry LMSAC, Mohamed 1st University, Oujda, Morocco; [c]Department of Chemistry, An-Najah National University, Nablus, Palestine; [d]Laboratory of Applied Sciences, National School of Applied Sciences d'Al-hoceima, Abdelmalek Essaadi University, Tétouan, Morocco

ABSTRACT

In the last decade calcium phosphate composites and other related biomaterials, were commercially used for bone substitution or allografts. In this study, a method was developed for purpose. In this composite hydroxyapatite (HAp) was placed in a cellulose structure by dissolving and precipitation technique. The produced biocompatible composites were extensively characterized by means of Fourier-transform infrared spectroscopy, thermogravimetric analysis, powder X-ray diffraction, dynamic light scattering, and scanning electron microscopy. The analysis results showed that, Hap successfully included in cellulose network without affecting its crystallinity, or the properties of either cellulose or HAp. The analysis also revealed a strong physical interaction between the composite components. Therefore, the composite appears to be a useful for the fabrication of bioactive film that can be used in the Bone Tissue Engineering field. Novelty of this work is the synthesis of nanocomposites based on hydroxyapatite and cellulose to get nanomaterials by a new method of synthesis in organic chemistry, which is called the double decomposition method. This method creates patterns between the organic matrix and inorganic. The second object is to replace classical materials with new nanomaterials for medical and orthopedic uses.

GRAPHICAL ABSTRACT

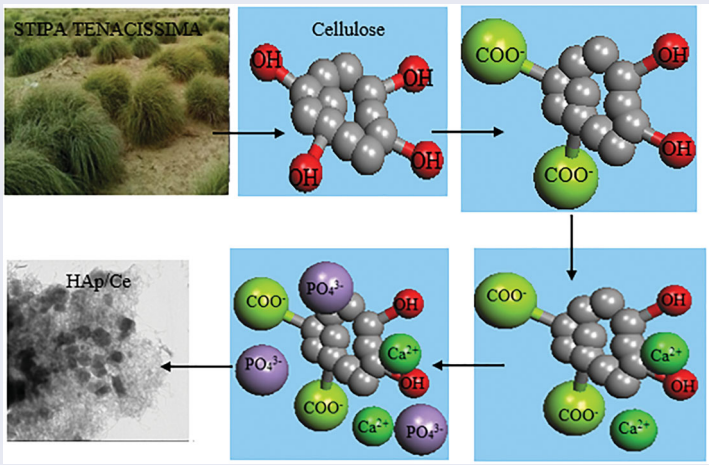

ARTICLE HISTORY
Received 22 October 2019
Accepted 1 February 2020

KEYWORDS
Calcium phosphate; cellulose; composite; hydroxyapatite; nanostructure; *Stipa tenacissima*

1. Introduction

Nano biocomposite materials have been studied in the last10 years as they are natural based and useful in medical applications as bone substitution[1,2]. Among the most used natural product as a base for biocomposite are polysaccharides, since they are biodegradable, biocompatible, nontoxic, and extracted from renewable sources[3]. Biopolymers are classified based on their origins plants, animals, or minerals[4]. They are extracted form fiber or powder. Generally, polysaccharides in fiber form such as cellulose are used in making thermoplastic composites[5,6,7].

CONTACT Shehdeh Jodeh sjodeh@hotmail.com Department of Chemistry, An-Najah National University, Nablus, Palestine; Khalil Azzaoui k.azzaoui@yahoo.com Department of Chemistry, Faculty of Sciences, Laboratory of Mineral Solid and Analytical Chemistry LMSAC, Mohamed 1st University, Oujda, Morocco.

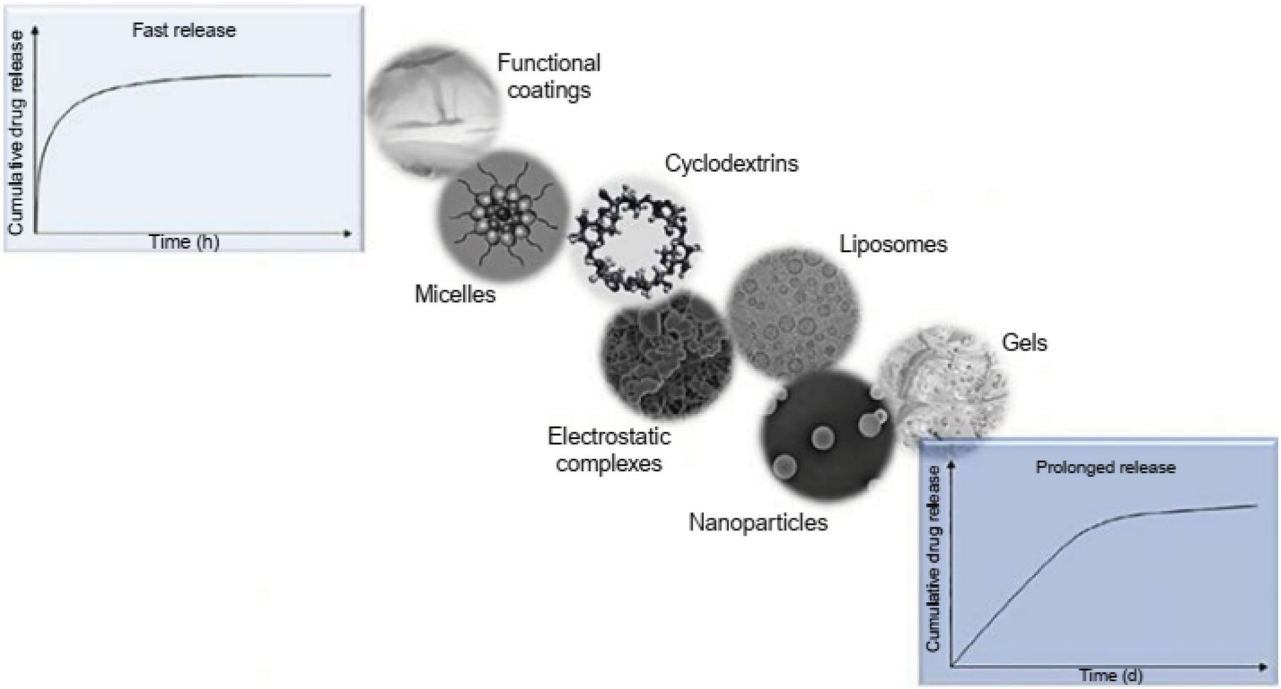

Figure 1. Hybrid nanocellulose-based cargo delivery systems[13].

Cellulose is a linear polysaccharide of (1–4) linked in β-D-glucose produced by almost all plants, algae, and some bacteria[3]. Cellulose are known to have unlimited number of useful number of applications, among these are cellulose-based magnetic materials, which are usually prepared by trapping iron oxides into a cellulose matrix[5]. The usefulness of magnetic nanocellulose (MNCs) was reported in several publications, for instance, it was used as in biomedical applications and as an oil adsorbent[8, 9]. Recently, a nanocomposite of cellulose nanocrystals (CNCs) and cobalt-iron oxide particles was used for making magnetic hybrid materials[10] from extraction of toxic dyes from wastewater.

Biomedical applications of nanocelluloses includes drug delivery and implants to tissue engineering and bioimaging and more[11,12] (Figure 1).

Biomedical applications of nanocelluloses usually requires adding a certain functional group and biological marker[14] to the cellulose structure. This could be done by a process known in the literature as chemical grafting. Examples on grafted cellulose are shown in Figure 2. Despite this large number of cellulose products, the number of products in the medical that reach the market is still limited, which could be attributed to drugs physical properties like lipophilicity or high molar mass especially in applications such as slow drug release and limited up-scale of production of large batches[15].

Other natural product that is useful in making biocomposites is hydroxyapatite (HAp)[16,17], which is a double salt of tricalcium phosphate and calcium hydroxide. Hydroxyapatite is a member of a large family of isomorphous substances. Hydroxyapatite is the principal inorganic ingredient of human bones and teeth, for this reason it gained a lot on interest and becomes a topic of extensive biological and physicochemical investigations (Narasaraju and Phebe 1996). It is often used as a main component of bone implant material[9] due to its chemical similarity to the natural calcium phosphate mineral present in biological hard tissues and is mainly used in the field of tissue engineering due to its excellent biocompatibility, bioactivity, non-inflammatory, nontoxicity, and osteoconductivity[18].

Several techniques for the preparation of hydroxyapatite are reported in the literature, among these are chemical precipitation[19], hydrothermal techniques[20] sol–gel, solid state, and mechano-chemical methods[21,22].

The synthesis of cellulose-hydroxyapatite gives as result a material combining the advantages of cellulose and Hap. The present work describes synthesis of new bio-composites based of cellulose and Hap. In first step, we report the synthesis of HAp and in the second step, we modified the cellulose with HAp.

The objective of this study is to synthesize ordered nanocomposites branched with CNCs and HAp. An SBF-based solution system was used to precipitate nanoscale HAp on the surface of branched CNCs. The size and distribution of the HAp crystals were studied and controlled by changing the reaction atmosphere, like T, pH, and molar ratio of calcium ions per functional groups on the CNC surface. In addition to study the transparent water-resistant coatings which was substituted on a substrate using casting the suspension of the nanocomposites and subsequent vapor-phase hydrothermal treatment. The unique nanocomposites could be the repeating units for functional materials in which are very useful for biomedical applications and strengthen mechanical properties of thin film.

2. Materials and methods

2.1. Material

All reagents and solvents used in this work were purchased for Aldrich chemical company and used as received without any further purification. The reagents include calcium nitrate

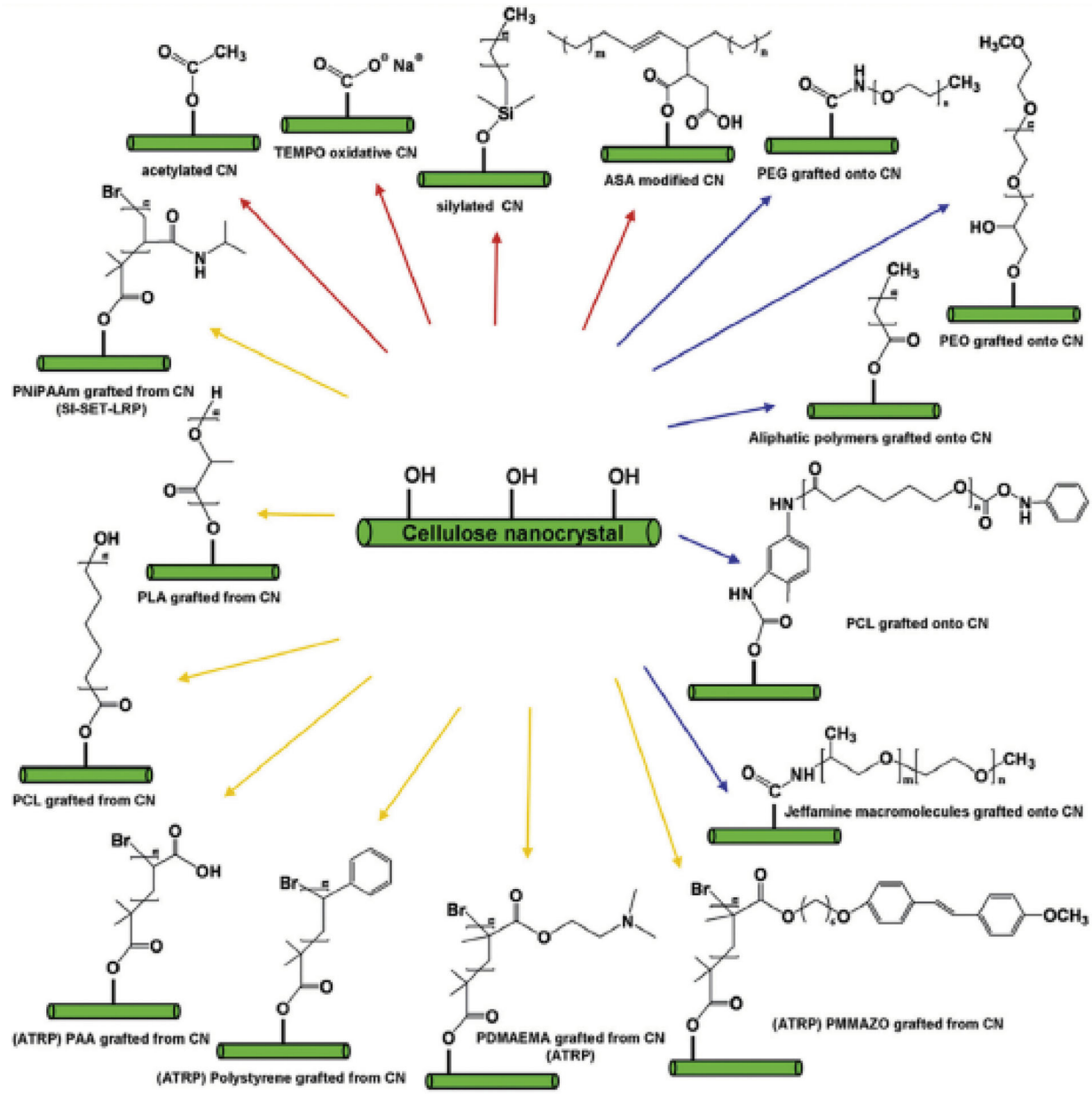

Figure 2. Schematic showing common surface modification reactions of cellulose nanocrystals (termed "CN" in the figure)[15].

$Ca(NO_3)_2{\cdot}4H_2O$ (99%), ammonium hydrogen phosphate $(NH_4)_2{\cdot}HPO_4$ (99%). Cellulose was extracted from Esparto "STIPA TENACISSIMA" of Eastern Morocco flowing a procedure developed by Elidrissi et al., using distilled water[23].

2.2. Isolation of cellulose

Esparto fibers has a cellulose content of about 500 mg/g that is contaminated by residual lignin and heteroxylans. It was purified by extraction of 1.0 g of Esparto fibers with 30 mL of glacial acetic acid (CH_3CO_2H, 80%) containing different concentrations of nitric acid (HNO_3) which was used as catalyst. This suspension of Esparto fiber in the acid solution was stirred for 2 h at 80 °C. Then the suspension was diluted by the addition of 20 mL of distilled water, filtered using suction vacuum, and then, rinsed several times with DW until we achieved neutral products after washing with ethanol. Net product which has almost cellulose was heated at 105 °C to achieve specific weight[23].

2.2.1. Preparation of cellulose solution

A 100 g of the solvent system that composed of 6% NaOH/, 4% Urea/,and 90% H_2O by weight was prepared[23]. To the solvent was added 2.0 g of the extracted cellulose and stirred. The product was kept in dry freezer and rinsed with crushed ice to obtain a transparent solution.

2.2.2. Preparation of nanocomposite based of cellulose/HAp

A 10 mL of cellulose (0.2 g) was placed in a three-nicked round flask with addition of solution of $Ca(NO_3)_2.4\,H_2O$ (1.88 g in 40 mL water) for 2 h with continuous stirring using a magnetic stirrer.

The suspension product was mixed for 20 min at a pH 10.5, then a 50 mL solution of $(NH_4)_2HPO_4$ (0.63 g in 50 mL

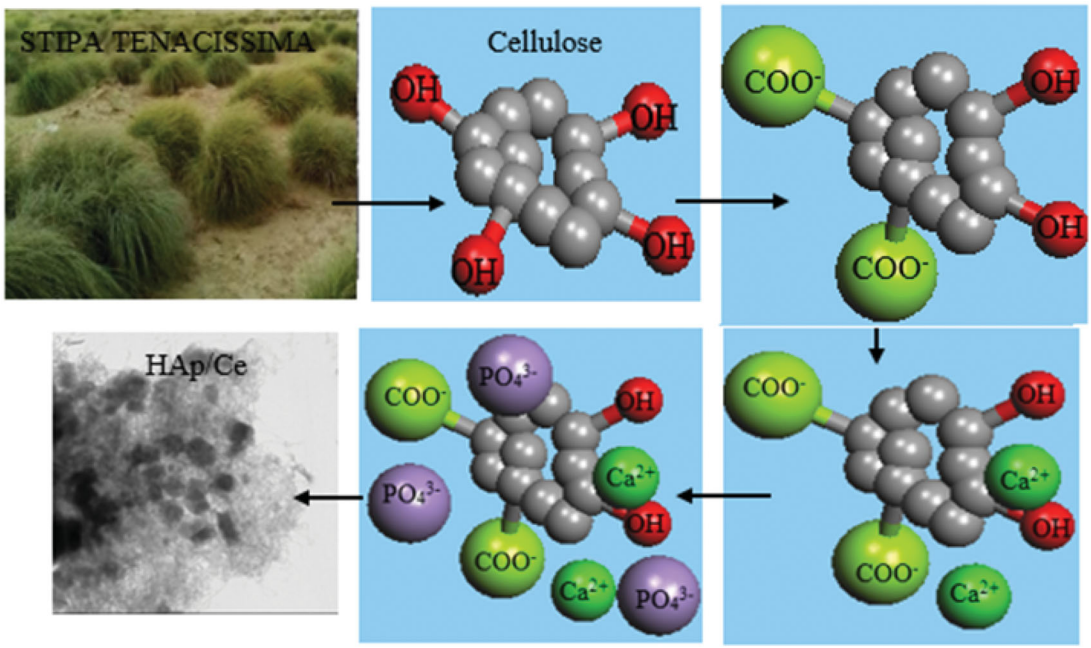

Figure 3. Illustration of cellulose extraction and HAp/Ce nanocomposite synthesis.

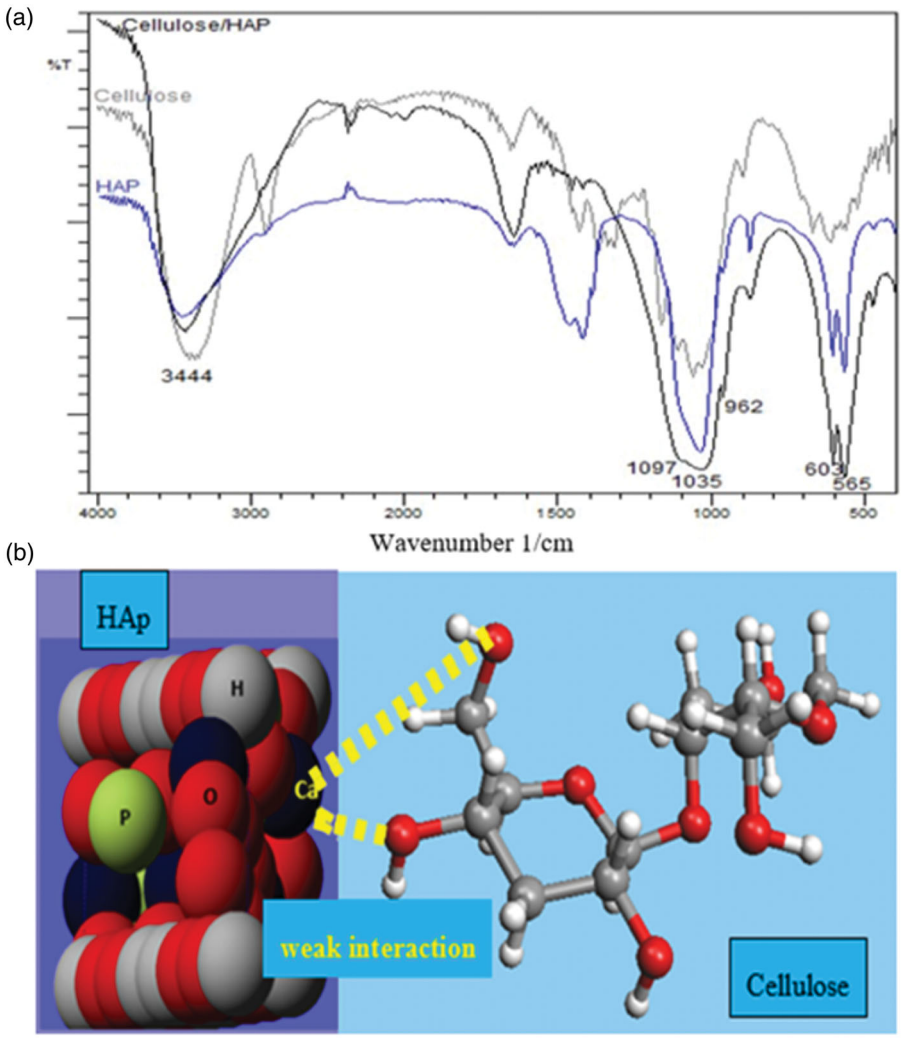

Figure 4. (a) FTIR spectrum of cellulose, HAp and HAp/Cellulose. (b) Schematic model shows the interaction between the OH groups of Ce and Ca^{2+} of hydroxyapatite.

water) maintained likewise at the same pH was placed in the funnel and were added dropwise to the reaction mixture. The temperature was increased to 80 °C and maintained for 90 min. The final product was separated by filtration, washing with hot distilled water to neutral pH, dried under vacuum at 80 °C for 24 h (Figure 3).

2.3. Characterization

The Fourier-transform infrared spectroscopy (FT-IR) spectroscopy was performed using a Shimadzu FT-IR 300 series instrument (Shimadzu Scientific Instruments). The following parameters were used: resolution was 2 cm^{-1}, spectral range was 400 cm^{-1} to 4,000 cm^{-1}, and number of scans was 128. The test samples were prepared by mixing 0.2 g of the nanocomposite with 0.8 g of KBr and a pellet was prepared from the sample.

The surface morphology of the composites was examined using scanning electron microscopy (SEM; SU 8020; Hitachi, Tokyo, Japan) at an acceleration voltage of 3.0 kV. The specimens were frozen under liquid nitrogen, fractured, mounted, coated with gold/palladium, and observed using an applied tension of 10 kV.

We analyzed the X-ray photoelectron spectra with the ACESS ESCA-V6.0F PHI software, and subsequently processed using the MultiPak 8.2 B software. The binding energy values were referenced to the C1 carbon signal casual (284.8 eV). To determine the binding energies, the Shirley bottom and the Gauss–Lorentz curves were used.

Standard thermogravimetric analysis (TGA) was performed using TGA Q500 and Q50 (TA Instrument), with a temperature range of 20–900 °C at a heating rate of 10 °C/min. The differential scanning calorimetry (DSC) curves were recorded on a DSC Q2000 V24.4 Build 116. Samples (10 mg each) were sealed in aluminum DSC pans and placed in the DSC cell. The apparatus Chromatography/mass spectrometry (GC-MS): A Shimadzu GCMS-QP2010 (Shimadzu, Japan) with GCMS solution 2.5 software.

2.3.1. Total organic carbon

The total organic carbon (TOC) analysis was performed in TOC/TN Analyzer multi N/C 2100/2100. The total carbon (TC) was used to represent the carbon present in the aqueous phase, Since the TC value covers all carbon (organic and inorganic) exist in the aqueous effluent, which is needed to close the carbon balance.

Muller–Hinton Broth (Biokar); Muller–Hinton Agar (Biokar); sterile paper discs; Potato Dextrose Agar (PDA); sterile distilled water; Petri dishes90 mm; Test Tubes.

2.3.2. Atomic force microscopy

The surface analysis was performed using the atomic force microscopy (AFM) to investigate the changes of the surface morphology of the mild steel after 6 h of immersion time at 303 K. The AFM measurements were carried out using VEECO CPII AFM.

2.3.3. Spectra of X-ray photoelectron spectroscopy

X-ray photoelectron spectroscopy (XPS) studies were analyzed using a Physical Electronic PHI 5700 spectrometer attached with a non-monochromatic Mg-Ka radiation (300 W, 15 kV, and 1,253.6 eV) for characterizing the core-level signals of the elements of our interest using a hemispherical multichannel detector. The detected spectra were analyzed using a constant pass energy value at 29.35 eV and 720 μm diameter circular analysis reagon.

2.3.4. ^{31}P NMR spectroscopy

Solid state ^{31}P nuclear magnetic resonance (NMR) was acquired using a high-resolution magic-angle spinning (MAS) on Bruker DRX-500 MHz spectrometer with 4 mm CP/MAS probe.

3. Results and discussion

As aforementioned, the objective of this research was to construct and characterize a biocompatible composite for Bone Tissue Engineering and repair. In this sense, a thermal stability study was performed on the composite to draw a clear picture on the interactions between composite components. For this reason, the composite was subjected to various analysis.

TABLE 1. A summary of the absorption bands of cellulose, Hap and Hap/Ce nanocomposites.

	Frequency (cm^{-1})	Assignments
	3,344	Stretching group of OH
Cell	2,910	Stretching vibration of –CH and–CH_2
	1,033	Deformation glycosidic C–O–C
	1,099	Stretching vibration of C–O
	3,410	O-H stretching
HAp	1,045	Asymmetric stretching of P–O
	962	Symmetric stretching of PO_4^{3-}
	601	phosphate being in vibration
	570	Deformation of O–P–O
	3,365	O-H stretching
	962	Symmetric stretching of PO_4^{3-}
	468	Deformation of O–P–O
HAp/Cell	565–603	Deformation of O–P–O
	1,097	Asymmetric stretching of P–O

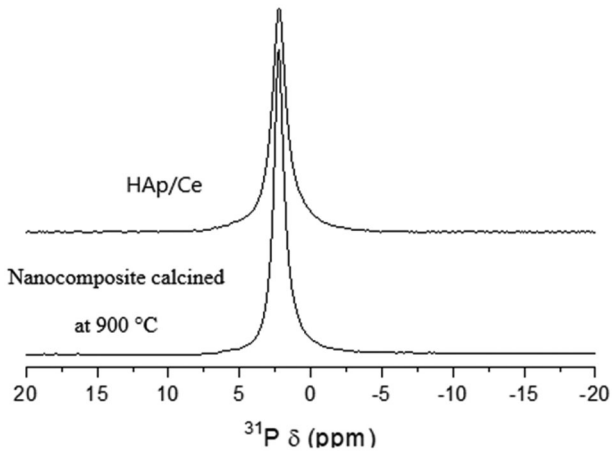

Figure 5. Plot of RMN, HAp/Ce, and HAp/Cellulose calcined.

3.1. FTIR analysis

The FTIR spectra of cellulose, Hap, and Nanocomposite of HAp/Cellulose are shown in Figure 4. The stretching bands observed in the FT-IR spectra of the three materials are summarized in Table 1. As shown in Table 1 and in Figure 4. The peak at 1,642 cm^{-1} could be due to the OH-bending vibration of adsorbed water. The composite has similar peaks to the starting materials expect there is some shift in the frequency of the main peaks. The O–H band, shift to higher wavelength than that for cellulose and the O–P–O showed as a broader band that extends from 565 to 603, and the P–O stretching band in the composite appear at 1,097 cm^{-1} while in HAp showed up at 1,045. The increase in the frequency of these band indicate the presence of interaction between the composite components.

A schematic model of the composite Hap/Cell is shown in Figure 4a, it could be used to explain the results obtained by ATR-FTIR, TGA/TDA,[31]P, and SEM, which suggest a strong interaction between the composite components. The schematic shows sites for complexation between Hap and Cell. As shown in the scheme, the interactions occurred between the OH groups of Cell and Ca^{2+} of hydroxyapatite.

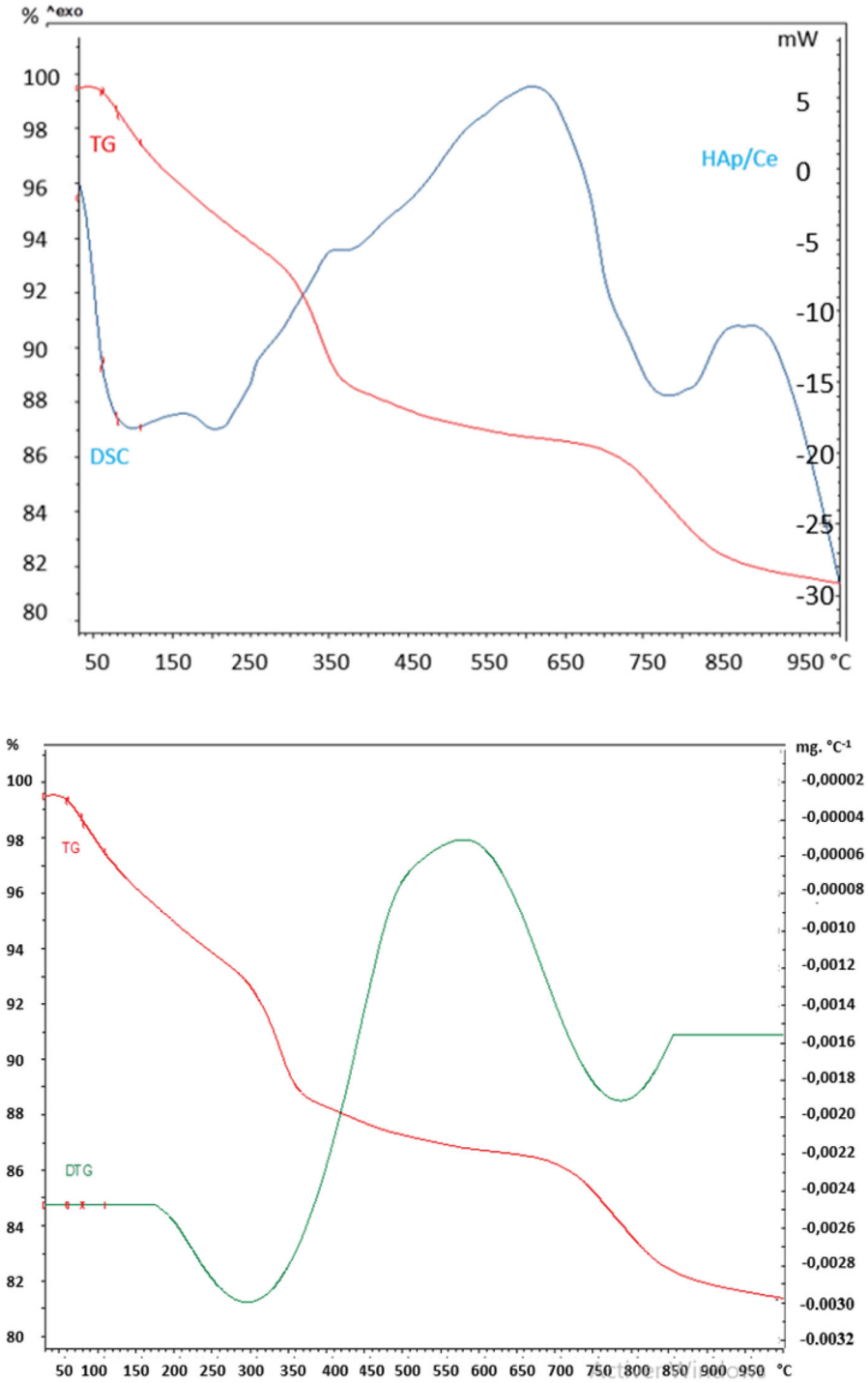

Figure 6. TGA/DTA thermograms of nanocomposite HAp/cellulose.

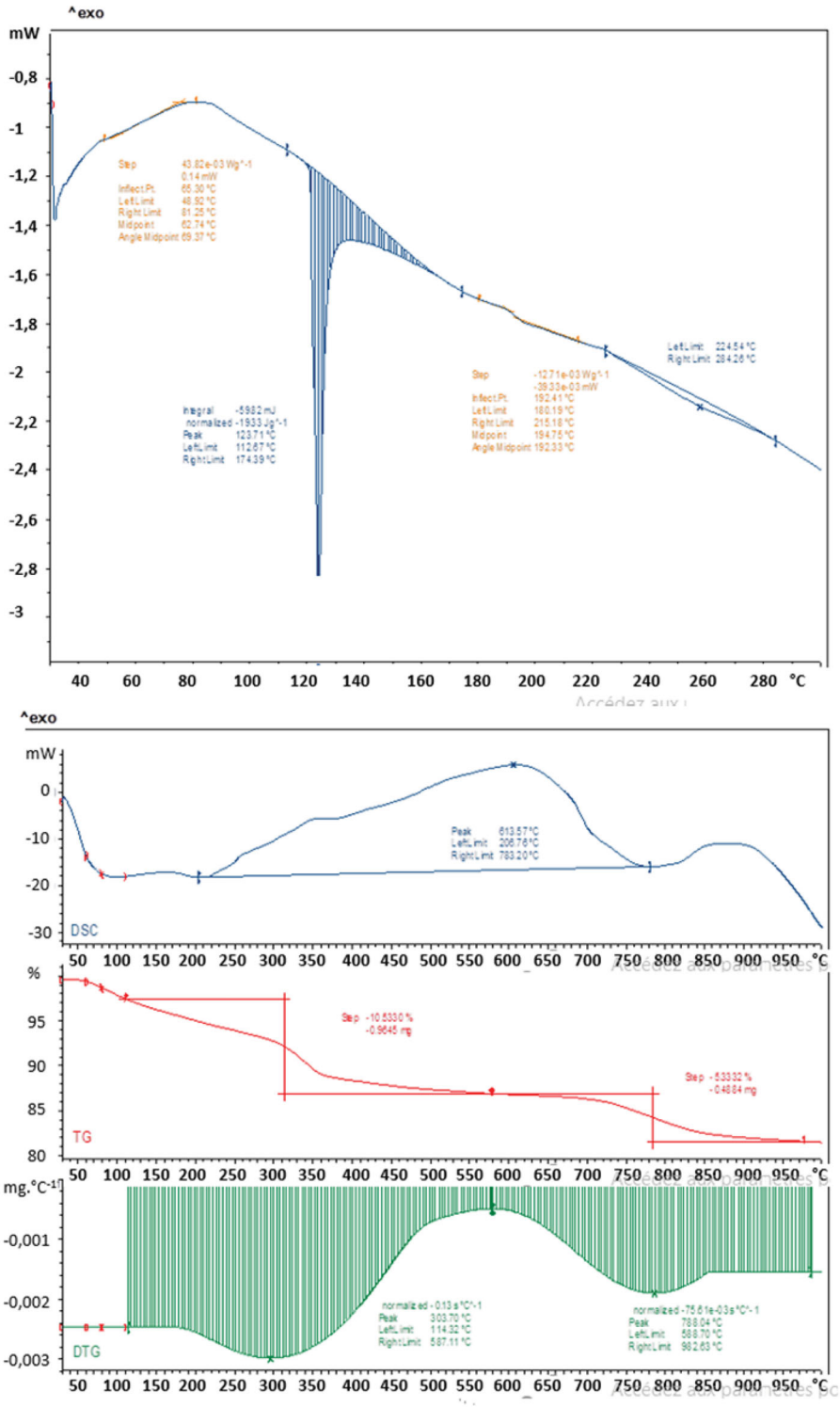

Figure 6. Continued.

The mechanism that lead to the complexation could be explained by the method of making the composites, which has four steps. In the first step the dissolution of the reagents in an aqueous medium; followed by the diffusion of water through the two matrices the organic the inorganic; formation of links between the functional groups of the composite components and formation of HAp/Cell composites (Figure 4b).

3.2. ^{31}P NMR spectroscopy

The solid state ^{31}P NMR spectra of Hydroxyapatite/cellulose and calcined hydroxyapatite-cellulose composite samples are shown in Figure 5.

Both spectra show a peak 2.1–2.6 ppm, which is typical for hydroxyapatite. However, they differ the peak intensity is different in the two spectra, due of the presence of amorphous region in calcined polymer.

3.3. Thermal analysis

The thermal properties of the HAp/Cell composites were determined by DSC and TGA, results are shown in Figure 6. The DSC thermogram shows two Tg points for the composite at 65 °C and 182 °C. The TGA diagrams (Figure 6) shows the weight loss (red line) and heat flow (green line) of the Hap-Cell composite. A temperature drop occurred at 315 °C which could be due to the thermal decomposition of the cellulose while the HAp decomposition started at about 725 °C. It is reported in the literature that, the decomposition of HAp occurs at three stage: (1) the formation of $Ca_{10}(PO_4)_6O_x(OH)_{2-2x}$ as a intermediate for the dihydroxylation and producing hydroxyapatite $Ca_{10}(PO_4)_6O$ (stage 2) followed with the decomposition of this hydroxyapatite (stage 3) and resulting calcium phosphates. T. Wang, A. Dorner-Reisel, and E. Muller, "Thermogravimetric¨ and thermokinetic investigation of the dihydroxylation of a hydroxyapatite powder," *Journal of the European Ceramic Society*. 24. 4. 693–698, 2004]. The first two stages can be observed at about 450 °C and 565 °C, respectively.

3.4. X-ray diffraction patterns of nanocomposite

To determine if any crystallinity loss occurred during the composite formation a X-ray diffraction (XRD) analysis was performed on the sample and the resulting pattern is Figure 7.

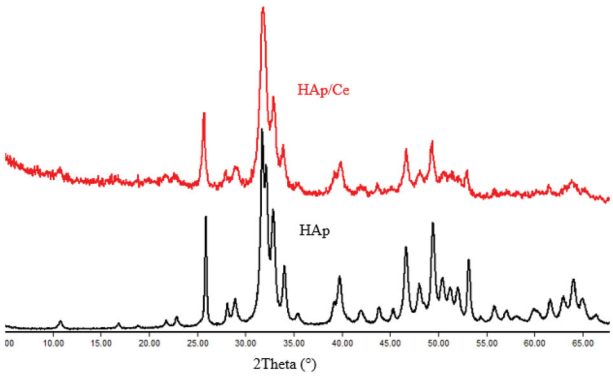

Figure 7. X-ray diffraction patterns of nanocomposite of HAp and HAp/Cell.

XRD was used to characterize the crystal phases of the prepared Hap and Cell/Hap composites. As shown in Figure 6, cellulose is known to show diffractions peaks at $2\theta = 10.9°$, 21.9°, 22.9°, 28.15°, and 35.5° which attributed to the crystalline polymorphic of cellulose II as reported by Klemm et al.[13]. The Hap shows sharps peaks at $2\theta = 25.98°$,31.89°,39.98°, 46.87°, and 48.6° corresponding to the lattice planes 002, 210, 211, 310, and 222 of HAP, (Figure 7), the peaks represent the high crystallinity of hydroxyapatite[8,24]. This results are in agreement with those obtained by Fu et al. and Azzaoui et al. It is clear that all diffraction patterns showed the same behavior except some broadening in some peaks. This show that the crystallinity of the sample was not lost after in the composite.

3.5. AFM analysis

The AFM is always used for qualitative and quantitative information about biopolymers at a nanometer scale which gives it an advantage over other techniques[25,26]. In this study, the AFM was used to characterize the surface characteristics of the HAp/Cellulose composite. The surface model of the composite is depicted in Figure 8. The figure shows a three-dimensional image of HAp/Cell composite in the scale of 0.9 and 6 µm. AFM images shows a smooth, roughness, and uniform surface.

3.6. Surface morphology

SEM was used to study the homogeneity of HAp/cell composite as shown in Figure 9a. In Figure 9b, the cellulose showed larger aggregate of plate shaped which was due to the agglomeration of these cellulose functionalized group which causes several interactions. During HAP mineralization, the cellulose morphology changed to more porous due to the presence of inorganic domains over the nanoparticles surface. The collision between cellulose-based nanomaterial and the cationic species (Ca^{2+} and PO_4^{3-}) leads to a solid and homogenous species with type of porosity. The analysis confirmed the presence of both calcium (Ca) and

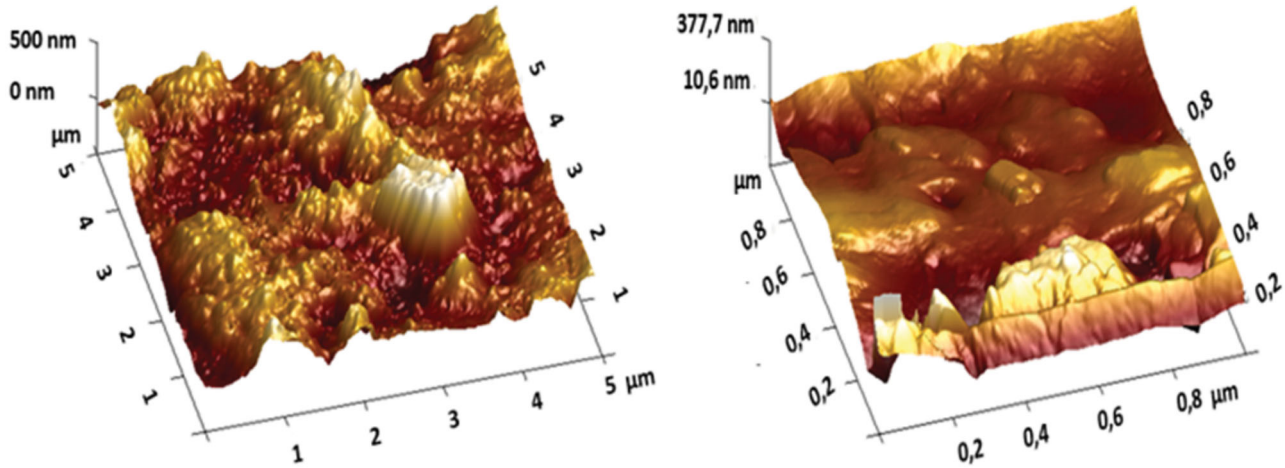

Figure 8. AFM micrographs of Hap/Cell surface at 1.0 g/L.

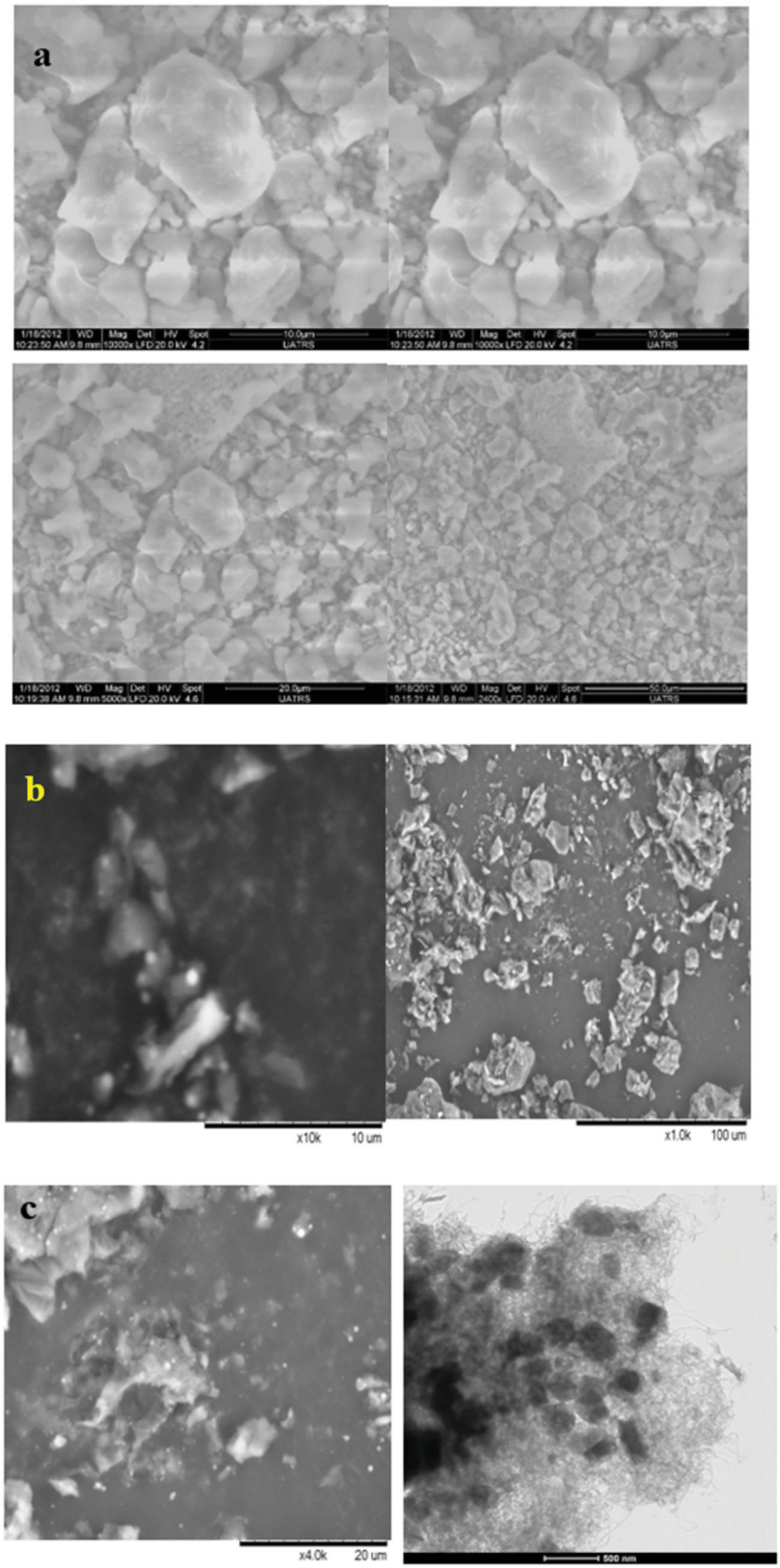

Figure 9. SEM/FEG images of (a) powder HAp. (b) Cellulose powder. (c) SEM/FEG images of HAp/Ce nanocomposite.

phosphorus (P). The last sample showed more porosity and multilayers of HAp above the surface. Such phenomena was showed by TGA data analysis. All images show a surface that is composed of spherical particles like grains with a nanoscale size and macropores with dimension ranged from 170 nm (Figure 9c).

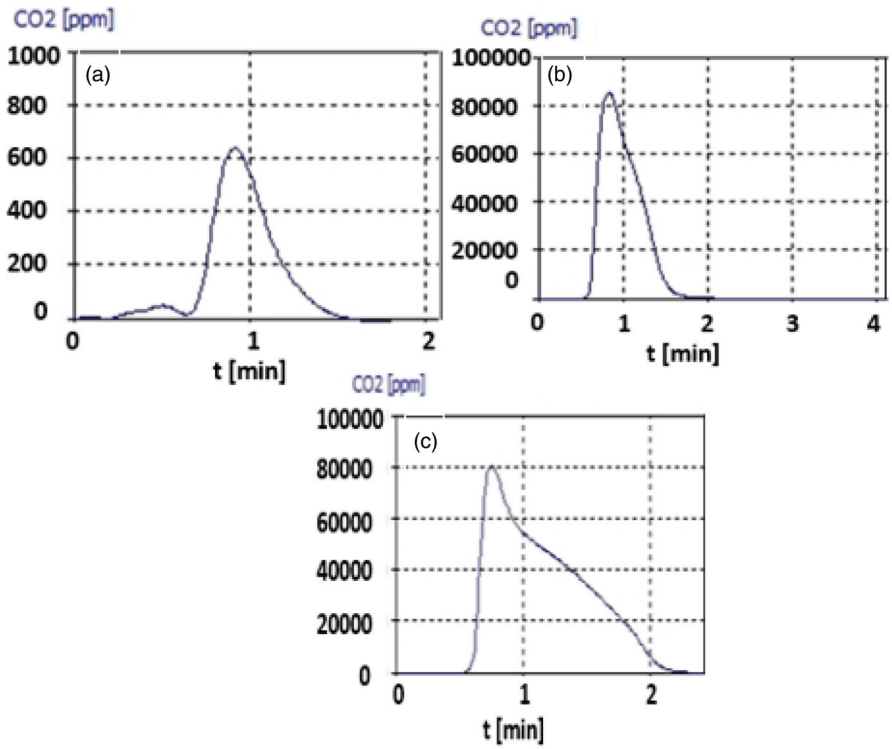

Figure 10. Plot of TOC versus time for (a) HAp, (b) Cellulose, and (c) HAp/Cellulose.

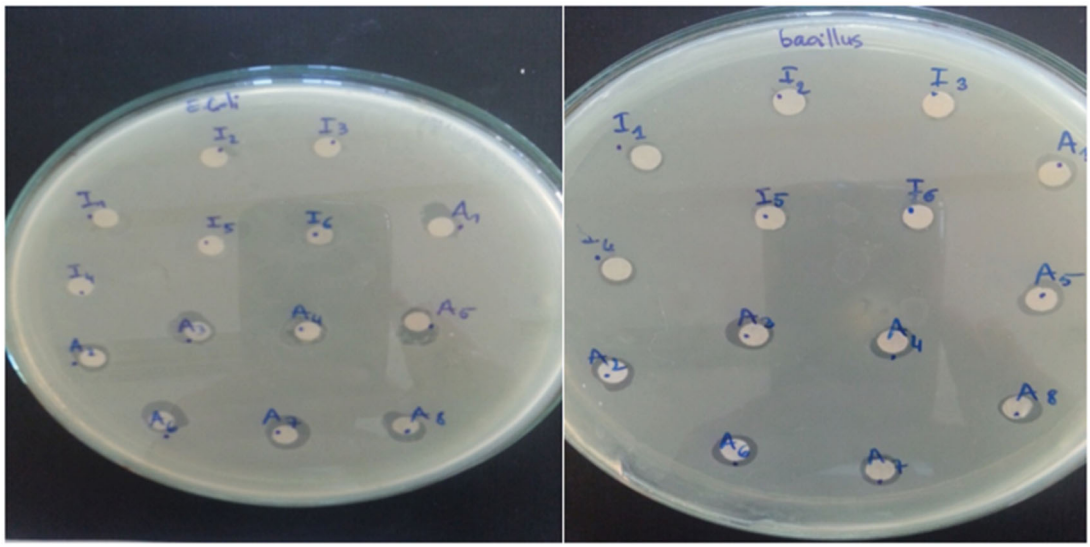

Figure 11. Sensitivity test in agar media.

Table 2. The diameter of inhibition of three composites with positive and negative control tested on three bacteria and one fungus.

Stains	HAp/Ce 40/50/10	HAp/Ce 30/60/10	HAp/Ce 20/70/10	C +	DMSO
B.S	9	9	9	26	–
M.L	9	–	–	27	–
E. coli	–	13	–	29	–
Candida	13	11	12	27	–

3.7. Total organic carbon production

Measurements of TOC indicated that carbon production from cellulose is higher than that of composites. As can see from the graph depicted in Figure 10, the amount of CO_2 produced from cellulose present in the composite was reduced by about 20%. The CO_2 in the composite was lost a longer period of time indicating the cellulose stability in the composite.

3.8. Antibacterial and antifungal test

The antimicrobial properties of the prepared composite was evaluated against three bacterial strains (*Bacillus Subtilis*, *Micrococcus luteus,* and *E. coli*) and a fungus (*Candida albicans*), results are shown in Table 2. The DMSO was used as a solvent, it showed no activities. Cycloheximide was also

evaluated as a control it showed a 27 mm diameter of inhibition against fungus organisms as shown in Figure 11. It also showed diameters of inhibition of 26–29 mm against *Micrococcus luteus* and 28 mm against *E. coli* and *Bacillus Subtilis*.

The test was carried out in an agar media, results show that, the HAp/cellulose nanocomposite with 40/50/10 wt. ratio respectively inhibited *Bacillus Subtilis* (B.S) and *Micrococcus luteus* (M.L) with a diameter of inhibition of 9 mm and showed a higher inhibition against *Candida albicans* (12 mm) as shown in Figure 11.

The nanocomposite30/60/10 (HAp/cellulose) also demonstrated antibacterial activity against *Bacillus Subtilis* (B.S) and *E. coli* with a diameter of inhibition of 9 and 13, respectively. It also showed activity against the fungus *Candida albicans* with a 11 mm diameter of inhibition.

As shown in Table 2, all tested composites showed antifungal activities. The highest inhibition was found for nanocomposite 40/50/10 weight ratio of HAp/cellulose. The antimicrobial activities was selective for some composites, nanocomposite with 20/70/10 of HAp/cellulose inhibited only the growth of bacillus.

4. Conclusion

Nanocomposite consisted of hydroxyapatite and cellulose as bone substitute biomaterial was developed. The HAp/Cellulose nanocomposite was synthesized using reprecipitation method by which the samples were mixed. As showed by various analysis methods such as the XRD, TGA, DSC, FT-IR, and others cellulose included Hap in its network without affecting its crystallinity, or the properties of either cellulose or HAp. A strong physical interaction occurred between them. Finally, the study showed that HAp nanocomposite can be used for the fabrication of bioactive film which has several applications in the Bone Tissue Engineering field. The object is to replace classical materials with new nanomaterials for medical and orthopedic uses. The results suggest that the HAp/Cellulose nanocomposite is a potential candidate for bone regeneration and bone reparation.

Acknowledgments

The authors would like to thank both Mohammed Premier University and the Department of Chemistry at An-Najah National University for using their chemistry laboratories. The authors reported no funding for this manuscript.

Disclosure statement

No potential conflict of interest was reported by the author(s).

ORCID

S. Jodeh http://orcid.org/0000-0001-9074-0122

References

[1] Hansen, N. M. L.; Blomfeldt, T. O. J.; Hedenqvist, M. S.; Plackett, D. V. Properties of Plasticized Nanocomposite Films Prepared from Nanofibrillated Cellulose and Birch Wood Xylan. *Cellulose.* **2012**, *19*, 2015–2031. DOI: 10.1007/s10570-012-9764-7.

[2] Obadia, L.; Triaud, F.; Dupas, C.; Pilet, P.; Lamy, B.; Bouler, J. M.; Grimandi, G. Comparative Study of Physicochemicalof Calcium Phosphate Bone Substitutes. *ITBM-RBM.* **2005**, *26*, 312–318. DOI: 10.1016/j.rbmret.2005.10.002.

[3] Sirviö, J. A.; Kolehmainen, A.; Liimatainen, H.; Niinimäki, J.; Hormi, O. E. O. BionanocompositeCellulose-Alginate Films: Promising Packaging Materials. *Food Chem.* **2014**, *151*, 343–351. DOI: 10.1016/j.foodchem.2013.11.037.

[4] Bledzki, A.; Gassan, J. Composites Reinforced with Cellulose Based Fibres. *Prog. Polym. Sci.* **1999**, *24*, 221–274. DOI: 10.1016/S0079-6700(98)00018-5.

[5] Azzaoui, K.; Mejdoubi, E.; Lamhamdi, A.; Zaoui, S.; Berrabah, M.; Elidrissi, A.; Hammouti, B.; Fouda, M. M. G.; Al-Deyab, S. S. Structure and Properties ofHydroxyapatite/Hydroxyethyl Cellulose Acetate NanocompositeFilms. *Carbohydr. Polym.* **2015**, *115*, 170–176. DOI: 10.1016/j.carbpol.2014.08.089.

[6] Yabannavar, A.; Bartha, R. Biodegradability of Some Food Packaging Materials in Soil. *Soil Biol. Biochem.* **1993**, *25*, 1469–1475. DOI: 10.1016/0038-0717(93)90001-R.

[7] Hansen, N. M. L.; Plackett, D. Sustainable Films and Coatings from Hemicelluloses: A Review. *Biomacromolecules* **2008**, *9*, 1493–1505. DOI: 10.1021/bm800053z.

[8] Azzaoui, K.; Lamhamdi, A.; Mejdoubi, E.; Berrabah, M.; ELidrissi, A.; Hammouti, B.; Zaoui, S.; Yahyaoui, R. Synthesis of Nanostructured Hydroxyapatite in Presence of Polyethylene Glycol 1000. *J. Chem. Pharm. Res.* **2013**, *5*, 1209–1216.

[9] Azzaoui, K.; Lamhamdi, A.; Mejdoubi, E. M.; Berrabah, M.; Hammouti, B.; Elidrissi, A.; Fouda, M. M. G.; Al-Deyab, S. S. Synthesis and Characterization of NanocompositeBased on Cellulose Acetate and Hydroxyapatite Application to the Absorption of Harmful Substances. *Carbohydr. Polym.* **2014**, *111*, 41–46. DOI: 10.1016/j.carbpol.2014.04.058.

[10] Lakrat, M.; Azzaoui, K.; Jodeh, S.; Akartasse, N.; Mejdoubi, E.; Lamhamdi, A.; Berrabah, M.; Hamed, O.; Razzouki, B.; Algarra, M.; et al. The Removal of Methyl Orange by Nanohydroxyapatite from Aqueous Solution: Isotherm, Kinetics and Thermodynamics Studies. *Desalin Water Treat.* **2017**, *85*, 237–249. DOI: 10.5004/dwt.2017.21260.

[11] Lin, N.; Dufresne, A. Nanocellulose in Biomedicine: Current Status and Future Prospect. *Eur. Polym. J.* **2014**, *59*, 302–325. DOI: 10.1016/j.eurpolymj.2014.07.025.

[12] Sunasee, R.; Hemraz, U. D.; Ckless, K. Cellulose Nanocrystals: A Versatile Nanoplatform for Emerging Biomedical Applications. *Expert Opin. Drug Deliv.* **2016**, *13*, 1243–1256. DOI: 10.1080/17425247.2016.1182491.

[13] Klemm, D.; Heublein, B.; Fink, H.-P.; Bohn, A. Cellulose: Fascinating Biopolymer and Sustainable Raw Material. *Angew. Chem. Int. Ed.* **2005**, *44*, 3358–3393. DOI: 10.1002/anie.200460587.

[14] Hua, K.; Rocha, I.; Zhang, P.; Gustafsson, S.; Ning, Y.; Strømme, M.; Mihranyan, A.; Ferraz, N. Transition from Bioinert to Bioactive Material by Tailoring the Biological Cell Response to Carboxylated Nanocellulose. *Biomacromolecules.* **2016**, *17*, 1224–1233. DOI: 10.1021/acs.biomac.6b00053.

[15] Lin, N.; Huang, J.; Dufresne, A. Preparation, Properties and Applications of Polysaccharide Nanocrystals in Advanced Functional Nanomaterials: A Review. *Nanoscale.* **2012**, *4*, 3274–3294. DOI: 10.1039/c2nr30260h.

[16] Jodeh, S.; Hamed, O.; Melhem, A.; Salghi, R.; Jodeh, D.; Azzaoui, K.; Benmassaoud, Y.; Murtada, K. Magnetic Nanocellulose from Olive Industry Solid Waste for the Effective Removal of Methylene Blue from Wastewater. *Environ. Sci.*

Pollut. Res. **2018**, *25*, 22060–22074. DOI: 10.1007/s11356-018-2107-y.

[17] Azzaoui, K.; Mejdoubi, E.; Jodeh, S.; Lamhamdi, A.; Rodriguez-Castellón, E.; Algarra, M.; Zarrouk, A.; Errich, A.; Salghi, R.; Lgaz, H.; et al. Eco Friendly Green Inhibitor Gum Arabic (GA) for the Corrosion Control of Mild Steel in Hydrochloric Acid Medium. *Corros. Sci.* **2017**, *129*, 70–81. DOI: 10.1016/j.corsci.2017.09.027.

[18] Murugan, R.; Ramakrishna, S. Bioresorbable Nanocomposite Bone Paste Using Polysaccharide Based Nano Hydroxyapatite. *Biomaterials.* **2004**, *25*, 3829–3835. DOI: 10.1016/j.biomaterials.2003.10.016.

[19] Kumar, A. S.; Kalainathan, S. Sol–Gel Synthesis of Nanostructured Hydroxyapatite Powder in Presence of Polyethylene Glycol. *Phys. B Phys. Condens. Matter.* **2010**, *405*, 2799–2802. DOI: 10.1016/j.physb.2010.03.067.

[20] Liu, H. S.; Chin, T. S.; Lai, L. S.; Chiu, S. Y.; Chung, K. H.; Chang, C. S.; Lui, M. T. Hydroxyapatite Synthesized by a Simplified Hydrothermal Method. *Ceram. Int.* **1997**, *23*, 19–25. DOI: 10.1016/0272-8842(95)00135-2.

[21] Toriyama, M.; et al. Synthesis of Hydroxyapatite-Based Powders by Mechano-Chemical Method and Their Sintering. *J. Eur. Ceram. Soc.* **1996**, *16*, 429–436. DOI: 10.1016/0955-2219(95)00123-9.

[22] Otsuka, M.; Matsuda, Y.; Hsu, J.; Fox, J. L.; Higuchi, W. I. Mechanochemical Synthesis of Bioactive Material: Effect of Environmental Conditions on the Phase Transformation of Calcium Phosphates during Grinding. *Bio-Med. Mater. Eng.* **1994**, *4*, 357–362. DOI: 10.3233/BME-1994-4502.

[23] El Idrissi, A.; El Barkany, S.; Amhamdi, H.; Maaroufi, A. K. Physicochemical Characterization of Celluloses Extracted from Esparto "*Stipa tenacissima*" of Eastern Morocco. *J. Appl. Polym. Sci.* **2012**, *23*, 537–547.

[24] Fu, L.-H.; Liu, Y.-J.; Ma, M.-G.; Zhang, X.-M.; Xue, Z.-M.; Zhu, J.-F. Microwave-Assisted Hydrothermal Synthesis of Cellulose/Hydroxyapatite Nanocomposites. *Polymer.* **2016**, *8*, 316. DOI: 10.3390/polym8090316.

[25] Elofsson, C.; Dejmek, P.; Paulsson, M.; Burling, H. Atomic Force Microscopy Studies on Whey Proteins. *Int. Dairy J.* **1997**, *7*, 813–819. DOI: 10.1016/S0958-6946(98)00008-9.

[26] Abdulkhani, A.; Hosseinzadeh, J.; Ashori, A.; Dadashi, S.; Takzare, Z. Preparation and Characterization of Modified Cellulose Nanofibers Reinforced Polylactic Acid Nanocomposite. *Polym. Test.* **2014**, *35*, 73–79. DOI: 10.1016/j.polymertesting.2014.03.002.

Abbreviations

HAp	Hydroxyapatite
Cel	Cellulose
MNCs	Magnetic nanocellulose
CN	Cellulosenanocrystals
TOC	Total organic carbon
DMSO	Dimethyl sulfoxide
M.L	*Micrococcus luteus*
E. coli	*Escherichia coli*
NMR	Nuclear magnetic resonance
FTIR	Fourier-transform infrared spectroscopy
DRX	X-ray crystallography
AFM	Atomic force microscopy
PDA	Potato dextrose agar
TC	Total carbon
XPS	X-ray photoelectron spectroscopy
B.S.	*Bacillus* Subtilis
SEM	Scanning electron microscope
31P	31Phosphorus NMR